Deriving the intermediate spectra and photocycle kinetics from time-resolved difference spectra of bacteriorhodopsin

The simpler case of the recombinant D96N protein

László Zimányi and Janos K. Lanyi
Department of Physiology and Biophysics, University of California, Irvine, California 92717 USA

ABSTRACT The bacteriorhodopsin photocycle contains more than five spectrally distinct intermediates, and the complexity of their interconversions has precluded a rigorous solution of the kinetics. A representation of the photocycle of mutated D96N bacteriorhodopsin near neutral pH was given earlier (Váró, G., and J. K. Lanyi. 1991. *Biochemistry*. 30:5008–5015) as $BR \xrightarrow{hv} K \leftrightarrow L \leftrightarrow M_1 \rightarrow M_2 \rightarrow BR$. Here we have reduced a set of time-resolved difference spectra for this simpler system to three base spectra, each assumed to consist of an unknown mixture of the pure K, L, and M difference spectra represented by a 3×3 matrix of concentration values between 0 and 1. After generating all allowed sets of spectra for K, L, and M (i.e., $M_1 + M_2$) at a 1:50 resolution of the matrix elements, invalid solutions were eliminated progressively in a search based on what is expected, empirically and from the theory of polyene excited states, for rhodopsin spectra. Significantly, the average matrix values changed little after the first and simplest of the search criteria that disallowed negative absorptions and more than one maximum for the M intermediate. We conclude from the statistics that during the search the solutions strongly converged into a narrow region of the multidimensional space of the concentration matrix. The data at three temperatures between 5 and 25°C yielded a single set of spectra for K, L, and M; their fits are consistent with the earlier derived photocycle model for the D96N protein.

INTRODUCTION

Proton transport by the halobacterial membrane protein bacteriorhodopsin is driven by changes of the pK_a of the retinal Schiff base and protein residues during relaxation of the light-induced *trans*-to-*cis* isomerization of the retinal $C_{13}—C_{14}$ double bond. The complex multicomponent reaction cycle ("photocycle") after absorption of the photon is reflected in spectral transformations of the chromophore and protein residues, as observed by visible as well as infrared and resonance Raman spectroscopy. Single turnover experiments at ambient temperature and low temperature spectroscopy of photostationary states have revealed the existence of six principal intermediate states labeled J, K, L, M, N, and O, with lifetimes ranging from picoseconds to milliseconds (reviewed recently in reference 1). Some of the transformations refer to transitions between isomeric states of the retinal (e.g., 2–4), whereas others, such as the L → M and the M → N reactions, refer to proton transfers between the Schiff base and aspartate residues (5–10). Thus, describing the reactions of the photocycle amounts to describing the reaction mechanism of the pump, and understanding the photocycle kinetics is an essential first step in understanding how the proton is transported.

Measurements of absorption changes at a few wavelengths in the visible have suggested that the intermediates arise and decay in a roughly sequential order (11). A large body of evidence indicates, however, that the kinetics are more complex than expected. For example, the rise and decay of the M intermediate is described not by two but by five or six relaxation times (12–16), inconsistent with a simple scheme containing only unidirectional reactions. To account for this, various photocycle models have been proposed over the last decade, with two or more bacteriorhodopsin subpopulations generating different photocycles (12, 14, 17, 18), branches before or after the M intermediate in the sequence (19–26), and a two-photon scheme (27). Single-wavelength measurements provided reliable information only about the kinetics of M (and perhaps O) because the absorption maxima of only these states and not the others are sufficiently removed from the maxima of bacteriorhodopsin and the rest of the intermediates. Unfortunately, data for one or two components could not decide, in principle, between alternative kinetic models. As it turned out, until recently multiwavelength measurements have not proved to be of practical advantage either. Strictly speaking, for data with low noise content, increasing the number of measured wavelengths beyond the number of intermediate states is redundant (28). More effort has been expended instead on describing the time constants of the reactions. Global analyses of absorption changes in the visible (29–33) and in the infrared (24, 34) have indicated that the photocycle contains five to seven relaxation times, with significant amplitudes at most wavelengths in the visible and many frequencies in the infrared. These phenomenological relaxation times, and the corresponding amplitudes, are functions of the desired elementary rate constants in the reaction sequence but in a complex and model-dependent way. To reconstruct the kinetics from this kind of cryptic data, both the extinctions of the components and the analytical solutions of all of the models to be tested would have to be known.

L. Zimányi's permanent address is Biological Research Center of the Hungarian Academy of Sciences, Szeged, Hungary.
Address correspondence to J. K. Lanyi.

0006-3495/93/01/240/12 $2.00

Despite these fundamental difficulties, a concensus is beginning to develop in favor of models consisting of single sequential photocycles with one or more reversible reactions to account for the observed complex kinetics (22, 23, 26, 32, 33, 35, 36). These schemes were derived not from unbiased global searches for a model but by the more conventional method of fitting intuitive models to complete or partial time-resolved data. The single sequential photocycle models are attractive in spite of this because they have inherent simplicity and self-consistency. Lozier and co-workers (36) chose the strategy of globally fitting a linear model containing one M and reversible reactions to time-dependent absorption changes at numerous wavelengths. This method yielded apparent elementary rate constants for transitions between spectral forms, but several of the spectra corresponded to mixtures of photointermediates based on what was known about the shape of the spectrum of the M intermediate. These authors concluded therefore that the model did not fully describe the photocycle and suggested that solution of the kinetics is possible only with additional information not contained in the measured spectra. We had come to the same conclusion but considered criteria for the shape and amplitude of the desired spectra as such additional information; using these as guidelines we arrived at the model, $BR \xrightarrow{h\nu} K \leftrightarrow L \leftrightarrow M_1 \rightarrow M_2 \leftrightarrow N \leftrightarrow O \rightarrow BR$ (plus an $N \rightarrow BR$ shunt) (23, 37). The main problem with this approach was the difficulty of deriving the spectra of the photointermediates from the difference spectra. Although the spectra generated with searches based on such criteria were reasonable and temperature invariant and the kinetics as well as the derived thermodynamics showed self-consistencies (35), the question of their uniqueness remained open.

This report is our attempts to (*a*) optimize the search for solutions in multidimensional parameter space and calculate the resulting intermediate spectra using first simulated and then real data, (*b*) explore the consequences of using various independent criteria to restrict the spectra and test the convergence of the solutions, and, finally, (*c*) evaluate the uncertainties in the spectra and the choice of models. We used the mutated protein D96N for this study because in its photocycle near neutral pH, the M decay is so slow that N and O do not accumulate significantly, and their contributions to the spectra and the kinetics can be neglected (23). The information provided by this simplified system is therefore on the first half of the photocycle. We find that in a search with simulated data, the solution averages strongly converge to the known solution. Two simple restricting criteria, i.e., requiring no negative absorptions and a single absorption band for the M intermediate, generate an average very near the correct solution. The further restricting criteria mostly reduce the standard deviations, i.e., the size of the solution space. Reassuringly, the search with the measured spectra appears to be convergent in a similar manner. We suspect that this method of spectral analysis may be of general validity and applicable for other systems as well, provided that the component spectra have strong predicted features. In this simple case at least, the principle of the calculation is valid and provides a robust solution defined by the available independent, but evidently mutually consistent, information about the shape of the component spectra. The results agree with the kinetic scheme $BR \xrightarrow{h\nu} K \leftrightarrow L \leftrightarrow M_1 \rightarrow M_2 \rightarrow BR$.

MATERIALS AND METHODS

D96N bacteriorhodopsin was purified as purple membrane (38) from *Halobacterium halobium* L-33 containing a recombinant *bop* gene with the asp96 to asparagine site-specific mutation described earlier (39). Time-resolved difference spectra were measured at the indicated temperatures ± 0.1°C, with the protein encased in polyacrylamide gels and equilibrated with buffer containing 100 mM NaCl, 50 mM phosphate at pH 8.0, and 2 mM NaN_3. The optical multichannel instrumentation and the nanosecond pulsed laser used for photoexcitation have been described before (40); the signal to noise ratio was improved over twofold through the use of a Glan-Thompson prism instead of a film-type polarizer in the measuring beam and a cylindrical lens in the laser beam.

Although the spectra contained originally 386 points, all matrix calculations were performed after reduction to 100 points. For the calculations, an AST 486/25 desktop computer (AST Research, Inc., Irvine, CA) was used with the SPSERV program (Dr. Csaba Bagyinka, Biological Research Centre of the Hungarian Academy of Sciences, Szeged, Hungary, H-6701) for singular value decomposition (SVD) noise filtering and spectral fittings. Programs written by L. Zimányi in Microsoft Basic PDS were used for the array searches and the integrations of the rate equations. The latter programs are available without charge from the authors to those interested.

RESULTS

Creating simulated data

To develop criteria for a search and to test its convergence, we performed the calculations with a set of difference spectra constructed from simulated component spectra with shapes and amplitudes similar to those derived earlier for K, L, and M from measured difference spectra of D96N bacteriorhodopsin (23). They were constructed from a measured spectrum of bacteriorhodopsin by shifting it (linearly on a wavenumber scale) and adjusting its amplitude. Because in the case of M this produced a narrower band than desired, we convoluted it with two Gaussian functions of different half-widths and combined the convolutions so as to approximate a realistic M spectrum. These simulated component spectra are shown in Fig. 1 *A* (*dashed lines*). A set of difference spectra ("data") was then generated by combining these spectra and that of bacteriorhodopsin, according to kinetics similar to that described earlier for D96N bacteriorhodopsin (23) shown in Fig. 1 *B* (*dashed lines*). As before (23, 37), the task was to derive the component spectra from the data, but now the solution, i.e., the in-

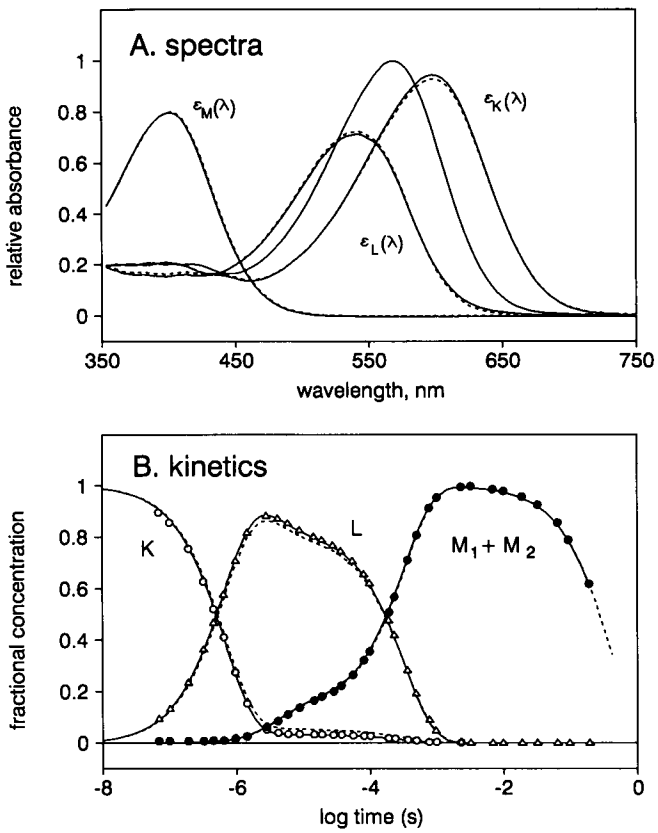

FIGURE 1 Input and calculated spectra (*A*) and kinetics (*B*) for simulated data. (*A*) *Dashed lines*, input spectra constructed as described in the text; *solid lines*, calculated average spectra after the third filter. The unlabeled spectrum is that of BR. (*B*) *Dashed lines*, input kinetics; *symbols*, calculated time-dependent concentrations of K (○), L (△), and M_1 plus M_2 (●); *solid lines*, best fit for the time-dependent concentrations. The rate constants (s^{-1}) were the following (input constants followed by calculated constants): k_{KL}, 1.37×10^6, 1.43×10^6; k_{LK}, 9.09×10^4, 5.56×10^4; k_{LM1}, 4.0×10^4, 4.0×10^4; k_{M1L}, 2.0×10^5, 2.0×10^5; k_{M1M2}, 2.0×10^4, 2.0×10^4; k_{M2BR}, 2.56, 2.56.

put spectra for K, L, and M and the kinetics, was known. Three subsets of difference spectra were chosen, from three time domains each with a large amplitude for at least one of the three component spectra. The third domain was well before three virtually time-invariant spectra, assuring that no recovery of the initial state had taken place. Each difference spectrum in these truncated data sets therefore contained the input spectra of K, L, and M with positive and variable amplitudes plus the bacteriorhodopsin spectrum with a negative and constant amplitude. Averaging within each of the time domains gave three difference base spectra as shown in Fig. 2 *A*. Adding the spectrum of the depleted bacteriorhodopsin gave the three absolute base spectra in Fig. 2 *B*. (We will describe below how the extent of the depletion was derived without using information on how the data were constructed.) In the analysis that follows, our aim was to see how well the original component spectra and kinetics could be regained from the data and to what extent the spectra have to be specified during the search to arrive at a solution within acceptable standard deviation of the input spectra.

Generating the solution array

An array containing all solutions was generated, and the solution space was progressively narrowed by applying restricting criteria for the calculated spectra of the intermediates as before (23, 37) but with a global grid-search. The rationale was as follows. If the three base spectra in Fig. 2 *B* are $\epsilon_1(\lambda)$, $\epsilon_2(\lambda)$, and $\epsilon_3(\lambda)$, and the unknown component spectra for K, L, and M are $\epsilon_K(\lambda)$, $\epsilon_L(\lambda)$, and $\epsilon_M(\lambda)$, then two vectors can be defined:

$$\vec{\beta}(\lambda) = \{\epsilon_1(\lambda), \epsilon_2(\lambda), \epsilon_3(\lambda)\}, \quad (1)$$

$$\vec{\epsilon}(\lambda) = \{\epsilon_K(\lambda), \epsilon_L(\lambda), \epsilon_M(\lambda)\}. \quad (2)$$

Since the three base spectra are linear combinations of the three component spectra it follows that

$$\vec{\beta} = \mathbf{A} \cdot \vec{\epsilon}, \quad (3)$$

where the matrix **A** contains the nine (unknown) amplitudes of the component spectra

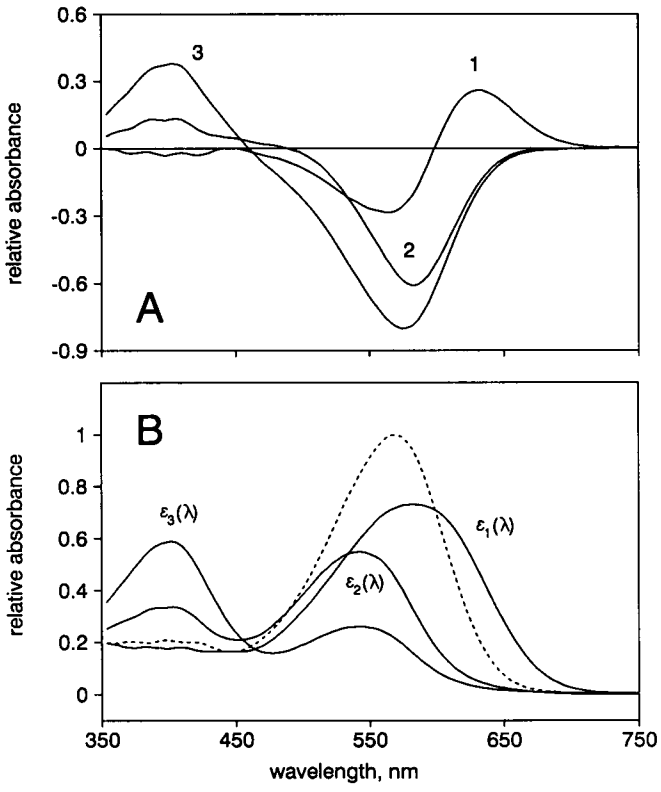

FIGURE 2 Base spectra from simulated data. (*A*) Difference base spectra, which are averages of difference spectra constructed from kinetics similar to that suggested earlier for D96N bacteriorhodopsin (23) between 70 and 940 ns (spectrum 1), 2.9 and 27 μs (spectrum 2), and 250 μs and 2.3 ms (spectrum 3), and normalized by 0.15 to 100% photoconversion. (*B*) Absolute base spectra designated as $\epsilon_1(\lambda)$, $\epsilon_2(\lambda)$, and $\epsilon_3(\lambda)$ in Eq. 1, obtained from spectra 1, 2, and 3, by adding the spectrum of bacteriorhodopsin (*dotted line*).

$$\mathbf{A} = \begin{pmatrix} a_{11} & a_{12} & a_{13} \\ a_{21} & a_{22} & a_{23} \\ a_{31} & a_{32} & a_{33} \end{pmatrix} \quad (4)$$

But since the spectra are scaled so that for each i

$$\sum_{j=1}^{3} a_{ij} = 1. \quad (5)$$

A has only six independent elements. The values of A can be represented by points in six-dimensional space whose coordinates assume values from 0 to 1. For the numerical calculations, these coordinates are divided into finite intervals that determine the grid density. The number of array points of A, at the grid density chosen, will be N. Each of the N points gives a spectrum for K, L, and M as follows:

$$\vec{\epsilon} = \mathbf{A}^{-1} \cdot \vec{\beta}. \quad (6)$$

Applying "filters" to restrict the size of the solution space

Each solution, corresponding to one of the N points in six-dimensional space, thus provides three component spectra. These spectra will assume all shapes allowed by the data, including a large number of incorrect ones. As in our earlier approach to this problem, the range of solutions is narrowed by eliminating those spectra that disobey successive restricting criteria. However, the calculation is now by an automated grid search that makes it possible to evaluate the results at each stage.

The number of grid points in a six-dimensional array is $(n+1)^6$, where $n+1$ is the number of resolved points on each coordinate, but since the sum of each row in matrix A must equal 1 (Eq. 5), the number of valid points will be $[(n+1)(n+2)/2]^3$. At a grid resolution of 1:50 ($n = 50$), it is $\sim 2.33 \times 10^9$. We reduced this number to $\sim 1.68 \times 10^7$ with the simple kinetic consideration of disallowing the amplitudes of the first component to increase and those of the third component to decrease. Thus, $a_{11} \geq a_{21} \geq a_{31}$ and $a_{13} \leq a_{23} \leq a_{33}$. This assigned the three columns in Eq. 4 to the amplitudes of the three-component spectra as they arise in time (by definition K, L, and M).

TABLE 1 **Location and distribution of the solution space represented by matrix A for simulated data after each of three filters that eliminate solutions with invalid spectra***

	First filter	Second filter	Third filter
a_{11}	0.716 ± 0.158	0.803 ± 0.140	0.670 ± 0.026
a_{13}	0.064 ± 0.050	0.017 ± 0.017	0.007 ± 0.010
a_{21}	0.031 ± 0.029	0.036 ± 0.032	0.020 ± 0.020
a_{23}	0.173 ± 0.048	0.223 ± 0.010	0.220 ± 0.000
a_{31}	0.015 ± 0.015	0.018 ± 0.016	0.010 ± 0.010
a_{33}	0.617 ± 0.024	0.641 ± 0.005	0.640 ± 0.000
N_s‡	1,987	163	16

* Since any one of the columns in matrix A is determined by the other two (Eq. 5), a_{i2} is left out of the table.
‡ Number of solutions.

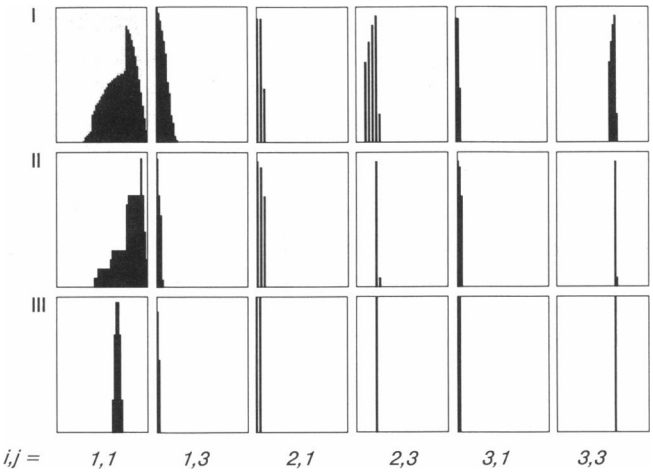

FIGURE 3 Shape of the solution space in the six-dimensional grid representing the values of matrix A. The distribution of solutions is shown as projections onto the six coordinates a_{ij} after the first (*top, I*), second (*middle, II*), and third (*bottom, III*) filters. The scales of the coordinates are not shown for clarity; for the ordinate (number of solutions at each value of a_{ij}) they were adjusted individually to allow comparison of all the patterns; for the abscissa (values of a_{ij}) they are from 0 to 1 uniformly.

The first filter consisted of applying the following two criteria: (*a*) negative absorption disallowed and (*b*) a second maximum in the M spectrum disallowed. The first criterion is self-evident. The second is based on the idea that the strongest excited states of the retinal chromophore (which produce the intense broad absorption band, near 410 nm in the case of the M state) are the lowest-lying ones (41). Indeed, at 234°K where all of the sample was photoconverted to M, the spectrum in the visible contained no bands on the long wavelength side of the 410 nm maximum (42). The input M spectrum had been constructed with this in mind. Although the data were virtually noise free, noise anticipated in actual data (cf. below) was taken into account in case *a* by rejecting spectra that contained a negative amplitude > 0.005 at any wavelength. In case *b* the spectrum of M was averaged between the highest measured wavelength and a wavelength where the amplitude of a Gaussian curve of the same bandwidth would be 2.5% of its maximum. Spectra in which this averaged amplitude was >0.002 were rejected. These numerical values were between ones that gave no solutions, and others that returned many M spectra we judged to be distorted.

The first filter turned out to be unexpectedly powerful. It lowered N_s (the number of grid-points yielding solutions, i.e., accepted spectra) to 1,989. The averages and standard deviations of the array parameters at this stage are given in Table 1. These numbers give information about the size of the solution space and its approximate shape. Fig. 3 shows additionally the distribution of solu-

tion array points on each grid line of the six coordinates a_{ij}. The ordinates in these graphs represent the number of accepted solutions, and the abscissae the values of a_{ij} ranging from 0 to 1. The distributions shown are thus the projections of the solution space onto the six coordinates. It is evident from Fig. 3 that the six-dimensional solution space is remarkably compact even after the first filter. Most of the roughness in its shape, as in the projections onto the a_{21} and a_{23} coordinates, is due to the finite grid density used and would have been eliminated at a finer resolution. As Fig. 3 shows, the overall shape of the solution space changed little as its size became smaller when further filters (cf. below) were applied.

Figure 4 *A* shows the spectra for K, L, and M calculated from the matrix element averages. The shaded areas are between spectra calculated from the set of matrix elements that lie ±1 SD away from the means. The spectrum of M is virtually completely defined by this filter and those of K and L are considerably restricted both with respect to shape, maximum, and amplitude. It is evident that the average spectra for K, L, and M are similar already at this stage to the input component spectra (compare spectra in Fig. 4 *A* to Fig. 1 *A, dashed lines*).

In difference spectroscopy the fraction of the photoexcited chromophore, which determines the amplitude of the (negative) contribution of bacteriorhodopsin to the measured difference spectra of the base spectra, is usually not known. We anticipated, however, that during the grid search we would obtain this parameter because a calculated M spectrum with no features above ~500 nm would not be obtained unless the correct amount of bacteriorhodopsin is added. Amounts too small would give negative absorption in this region and therefore no solutions. Amounts large enough to give solutions but not of the correct magnitude would generate difference bands with positive or negative lobes because the spectrum of bacteriorhodopsin cannot be reproduced by any sum of accepted spectra for K and L. The shape of the calculated spectra for M as various likely photocycling fractions were used to generate the absolute base spectra from the difference base spectra (cf. Fig. 2, *A* and *B*) indicated that there was a single photocycling ratio, 15.0%, where the spectrum of M had less distortion than at any lower or higher photocycling ratio (Fig. 5 *A*). How well this value is defined by the shape of the M spectra depends on the signal to noise ratio; with the simulated data the precision was about ±0.1%. The actual ratio used to create the data was in fact 15.0%.

The second filter was based on the idea that the higher excited states, which produce the indistinct and overlapping absorption bands below 450 nm in chromophores containing a protonated Schiff base, are covalent rather than ionic in character and should not be affected by changes in electronic configuration near the retinal (43). Thus, the amplitude in this wavelength region will be

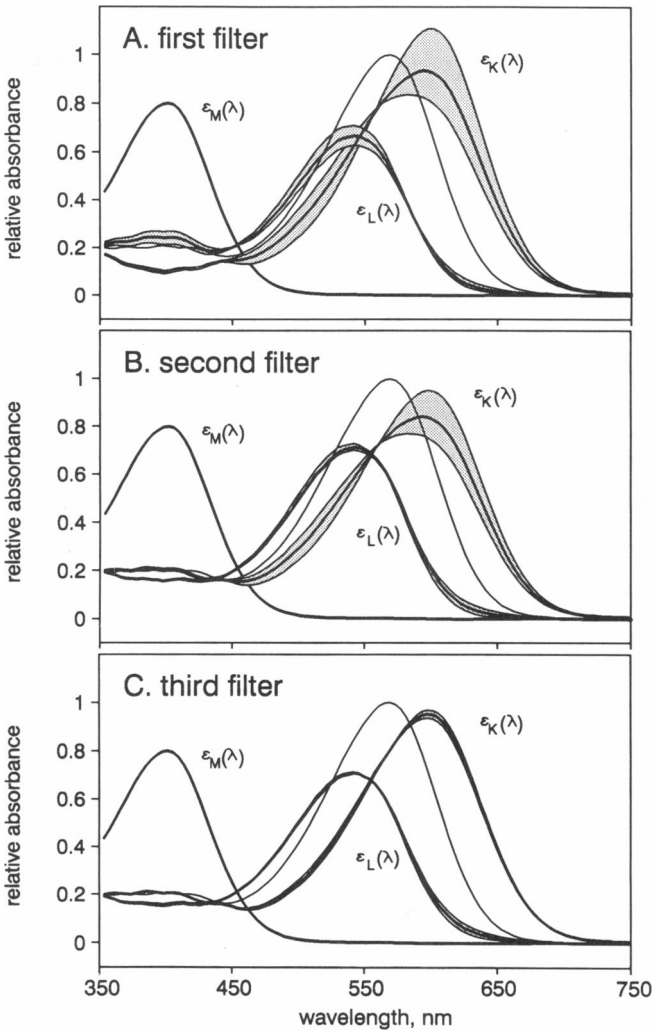

FIGURE 4 Calculated component spectra for simulated data, after the three filters (*A, B,* and *C,* respectively) discussed in the text. The spectra of K, L, and M, designated as $\epsilon_K(\lambda)$, $\epsilon_L(\lambda)$, and $\epsilon_M(\lambda)$, respectively, are calculated from the matrix elements in Table 1. The averages are shown as bold lines; the shaded areas are between two spectra calculated with all of the matrix values set to the averages plus the standard deviations and the averages minus the standard deviations. For the M spectra this range was too narrow to illustrate. In each panel the spectrum of bacteriorhodopsin is also included.

invariant in BR, K, and L. This is evidently less so for K than for L, since absorption near 400 nm decreases somewhat on K formation (e.g., Fig. 3 *A* in reference 15 and measured difference spectra below). The input spectra (Fig. 1 *A, dashed lines*) had been constructed to include these considerations. Anticipated noise in the measurements was allowed for by rejecting only those spectra for which the averaged amplitudes between 360 and 420 nm lay outside the range of ±25% of the amplitude of BR in this region for K and ±10% for L. This procedure reduced the number of solutions to 163. Their averages and standard deviations are given in Table 1. Fig. 4 *B* shows that the spectra calculated from the matrix averages were not greatly changed relative to the spectra after

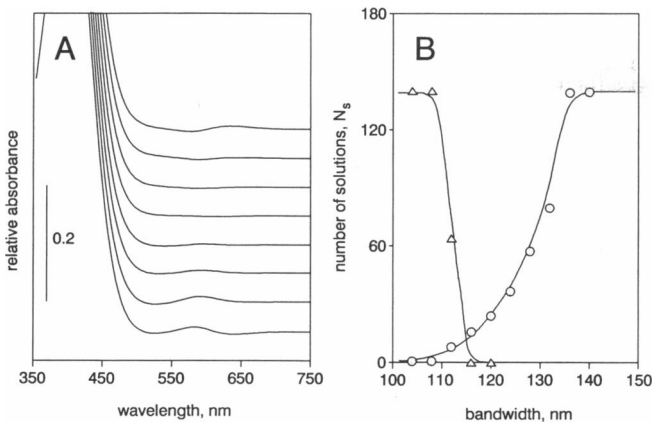

FIGURE 5 (*A*) Dependence of the calculated spectrum of M on the assumed fraction of photocycling bacteriorhodopsin. The spectra were calculated with base spectra from the simulated data such as in Figure 2 *A* but generated by normalizing with various amounts of photoconversion. The spectra, beginning with the uppermost, were calculated with 14.6, 14.8, 14.9, 15.0, 15.1, 15.2, 15.4, and 15.6% photocycling ratio. The number of solutions, N_s, were 220, 1,082, 1,251, 1,989, 1,311, 1,794, 452, and 286, respectively. At 14.4% photocycling ratio, no solutions were found. (*B*) Dependence of the number of solutions on the allowed minimum (△) and maximum bandwidths (○) for the calculated component spectra after the second filter (cf. text). Solutions were rejected when the spectrum of either K or L had a bandwidth less than or greater than indicated.

the first filter. Several of the standard deviations in Table 1, particularly those that affect the spectrum of L, were reduced, however.

The third filter was based on the amplitudes and bandwidths of the spectra. There is good reason to believe that the absorption amplitudes of all 13-*cis* retinal containing chromophore configurations will not exceed those of the all-*trans* retinal chromophores. It is that the transition dipole moment depends on the end-to-end distance of the extended π-orbital of the conjugated retinal chain, and rotation around any one of the C—C bonds brings the ends of the chain closer than in the fully extended all-*trans* isomer. The component spectra (Fig. 1 *A, dashed lines*) contain this feature. Accordingly, all solutions containing K, L, or M spectra with amplitudes greater than the amplitude of BR were rejected. This reduced N_s to 140. The expected bandwidths of the spectra are, in general, less certain. Where measured or calculated, the spectral bandwidths (FWHM) of rhodopsins with protonated Schiff bases, from a large number of bacterial and vertebrate sources containing various retinal isomers, range from 100 to 116 nm at room temperature (e.g., 44–48). In using this kind of empirical criterion, it is reassuring that low temperature spectra of the bacteriorhodopsin intermediates (42) do not reveal unusual amplitudes or shapes. The bandwidths of the input spectra K and L (Fig. 1 *A, dashed lines*) were 111 and 103 nm, respectively. Since the spectrum of M was already determined by the first filter, we excepted its spectrum from these calculations. As shown in Fig. 5 *B*, the dependency of the number of solutions on the minimal and maximal allowed bandwidths indicated that all K and L spectra calculated after the first two filters had bandwidths >104 nm and <136 nm. We limited the maximal bandwidth to 116 nm. This and the amplitude restriction constituted the third filter and reduced N_s to 16. The spectra for K, L, and M generated by the matrix averages and standard deviations (Table 1) after these calculations are shown in Fig. 4 *C*. The spectra are similar to those after the first two filters, as expected from the fact that the averages of the matrix elements remained within about one standard deviation throughout. The limits are much reduced, however. The final spectra for K, L, and M are nearly indistinguishable from the (known) component spectra (for this comparison, Fig. 1 *A* contains both input and final calculated spectra; *dashed* and *solid lines*, respectively). From these results, we draw the important conclusion that the original spectra can be retrieved from the over 10^9 array points without having to specify their shapes exactly. Remarkably, the criteria that decided the outcome of the calculation were the simplest: that the spectra cannot contain negative absorptions and M cannot contain a second maximum.

The statistics show that by applying the three consecutive filters the solutions strongly converge into a narrow region of the multidimensional space of the concentration matrix. Therefore, the solutions obtained are unique. Since the output spectra of K, L, and M, obtained by using the averages of the solution matrices, are almost indistinguishable from the input spectra, the solution average is the true solution. This means that there is no other set of physically acceptable absorption spectra that would reconstruct the three base spectra and thereby the entire set of initial difference spectra.

Kinetic fitting of the simulated data

The input difference spectra were resolved with a fitting routine into weighted sums of the calculated component difference spectra. This would test how well the original kinetics (Fig. 1 *B, dashed lines*) are regenerated by the calculated spectra. The weights of the components in the spectral mixtures gave their time-dependent concentrations, as shown by the symbols in Fig. 1 *B*. Up to 1 ms (i.e., before recovery of the initial state begins), the sums of the concentrations were within ±0.001 of 1 for each fitted spectrum, as expected. The rate constants returned from the best fit of the model (Fig. 1 *B, solid lines*) reproduced well those we used to create the data (cf. legend to Fig. 1). Thus, at least for data of this kind, the grid search method unambiguously and accurately returns the input kinetics.

In principle this analysis can be extended to include the second half of the photocycle in the wild-type system, provided that (*a*) it does not include more than one intermediate, as for example at high pH where the O intermediate does not accumulate, and (*b*) the time domain

is omitted where L and N (whose spectra are very similar) coexist (23). The kinetics of the first and second halves can be thus solved independently, with the K, L, and M spectra as unknowns in the first half and the M, N, and BR spectra as unknowns in the second half since repopulation of the initial state is with unknown kinetics also. Constancy of the photocycling amount and the calculated spectrum of M, as well as agreement with the known spectrum of BR, will be valuable restricting criteria in such an analysis.

Grid search with measured data

Time-resolved difference spectra were determined for D96N bacteriorhodopsin in the 70 ns to 420 ms time-range at 5, 15, and 25°C. Fig. 6 shows the measured spectra at 15°C up to 3.3 ms; these were used in all calculations except where otherwise indicated. We had established earlier (23) that under similar conditions the decay of M is so slow that the subsequent intermediates N and O do not accumulate to significant extents. This was confirmed by the fact that once the maximal amount of M was reached, all of the subsequent difference spectra (corresponding to the M minus BR spectrum) were virtually identical except in their amplitudes (last two spectra in Fig. 6 *C* and all the spectra that followed).

We assumed that this part of the photocycle contains only K, L, and M and that self-consistency of the solution would reveal in the end whether this assumption is justified. Singular value decomposition (49) treatment of the measured spectra gave a set of SVD spectra of which the first three had real features and the rest virtually only noise. By regenerating the original spectra from the first three or four SVD spectra, considerable noise reduction without loss of information was achieved (33). From the noise-filtered spectra, three sets were chosen for the averaging that produced the three base spectra; as for the simulated data in Fig. 2, the sets corresponded to delay times between 70 and 940 ns (first base spectrum), 4.2 and 170 μs (second base spectrum), and 250 μs and 3.3 ms (third base spectrum). These difference base spectra, as well as absolute base spectra calculated from them, are shown in Fig. 7, *A* and *B*.

The three filters used above for the simulated data effectively restricted the array for the measured data also and in a similar manner. As for the simulated data, the amount of photocycling bacteriorhodopsin was determined unambiguously after the first filter; it was 15.6% (± ~0.2%). The matrix elements and their standard deviations are given in Table 2; the calculated spectra and their standard deviations after the first filter are shown in Fig. 8 *A*. The distribution of solutions in six-dimensional space was similar to that calculated for the simulated spectra (not shown). After the first filter, N_s was 6,912. Table 2 and Fig. 8 *B* show that neither the matrix element averages nor the corresponding spectra were greatly changed after the second filter but N_s decreased to 286.

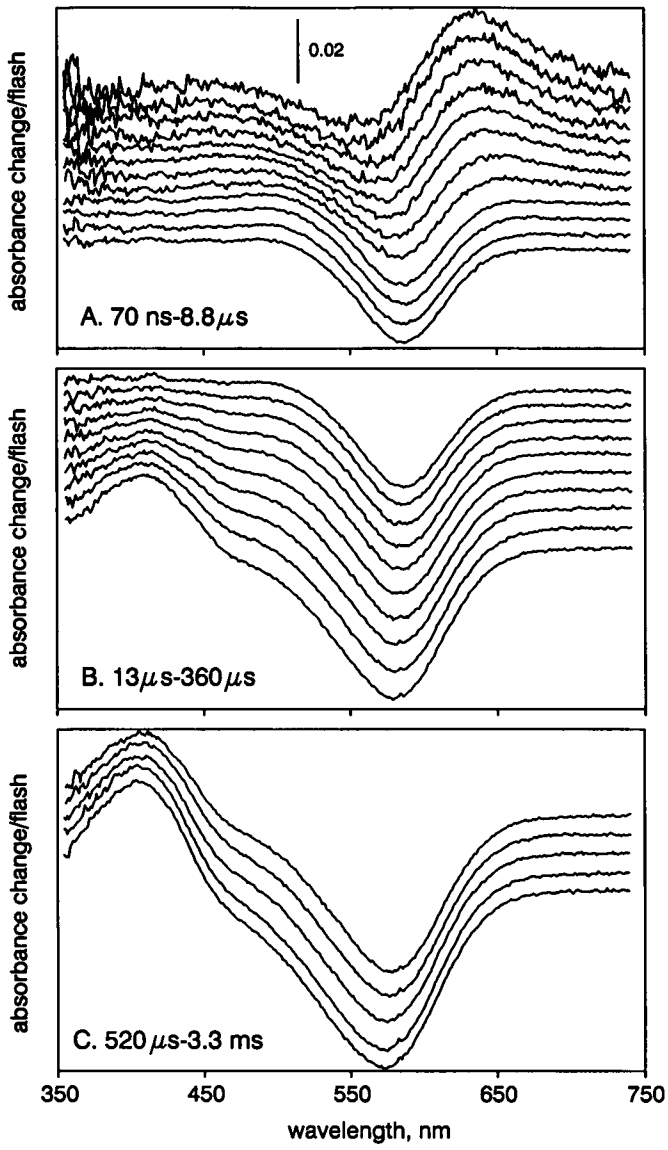

FIGURE 6 Measured time-resolved difference spectra for D96N bacteriorhodopsin. Conditions: 100 mM NaCl, 50 mM phosphate, pH 8.0, 2 mM NaN_3, 30 μM bacteriorhodopsin, 15°C. Delay times after photoexcitation (beginning with the uppermost traces in each panel): (*A*) 70 ns, 100 ns, 210 ns, 310 ns, 450 ns, 650 ns, 940 ns, 1.4 μs, 2.9 μs, 4.2 μs, 6 μs, and 8.8 μs; (*B*) 13 μs, 18 μs, 27 μs, 39 μs, 56 μs, 81 μs, 120 μs, 170 μs, 250 μs, and 360 μs; (*C*) 520 μs, 760 μs, 1.1 ms, 2.3 ms, and 3.3 ms.

After the second filter the spectral bandwidths of the calculated spectra were between 108 and 140 nm. In the third filter we restricted the amplitudes to 1 and the maximal bandwidths to 116 nm; this reduced the number of solutions to 18. The final matrix elements are given in Table 2; the corresponding calculated spectra are shown in Fig. 8 *C*. The way the spectra converged during this calculation greatly resembles the convergence with the simulated data (compare Table 1 with Table 2 and Fig. 4 with Fig. 8); for this reason we assume that here also the final spectra are close to the correct ones.

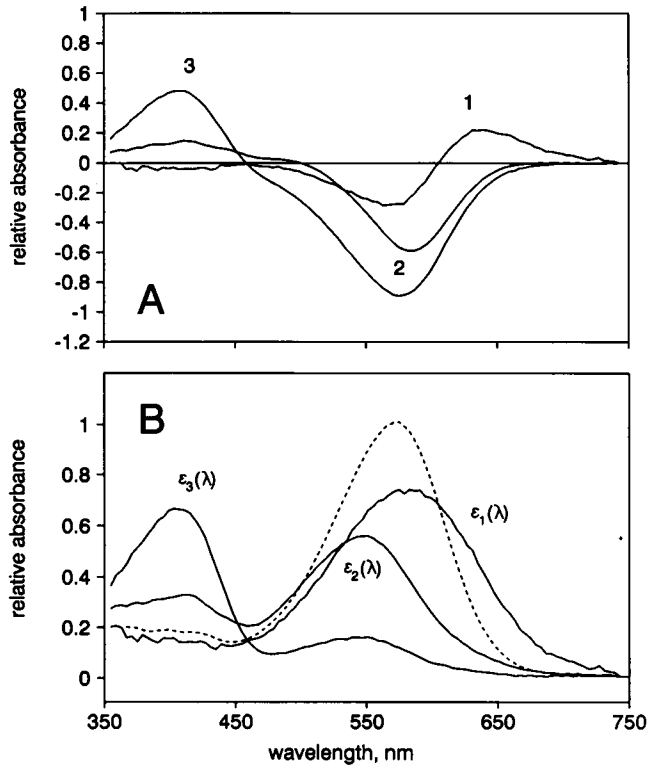

FIGURE 7 Base spectra from data at 15°C. (*A*) Difference base spectra, which are averages of SVD filtered measured spectra (cf. Fig. 6) between 70 and 940 ns (spectrum 1), 4.2 and 170 μs (spectrum 2), and 250 μs and 3.3 ms (spectrum 3), normalized by 0.156. (*B*) Absolute base spectra designated as $\epsilon_1(\lambda)$, $\epsilon_2(\lambda)$, and $\epsilon_3(\lambda)$ in expression 1, obtained from the spectra in *A*, by adding the spectrum of bacteriorhodopsin (*dashed line*).

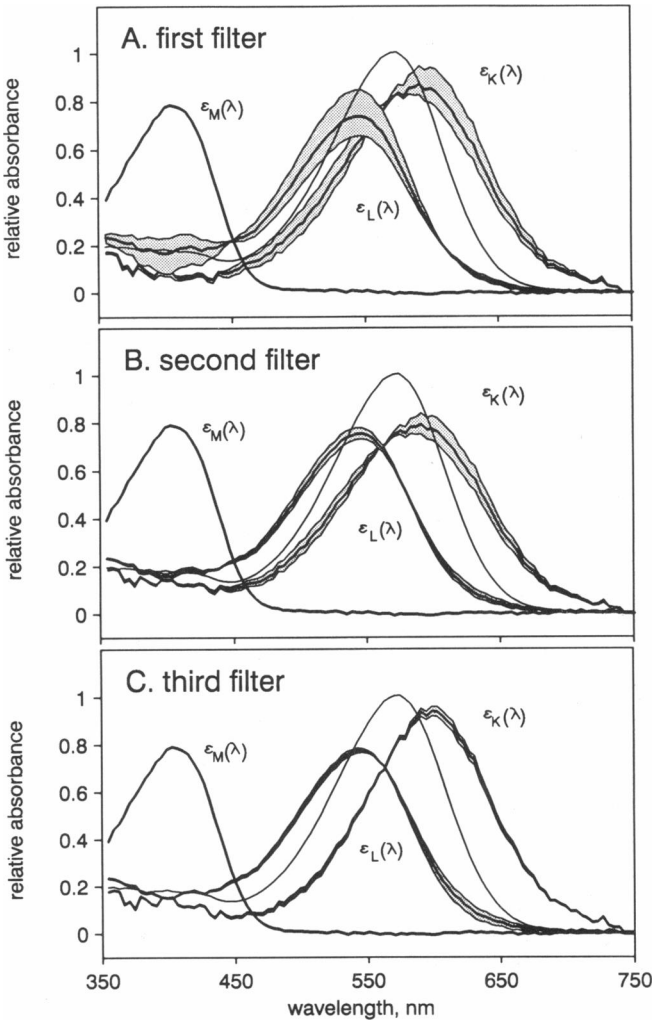

FIGURE 8 Calculated component spectra for D96N bacteriorhodopsin. The spectra of K, L, and M are designated as $\epsilon_K(\lambda)$, $\epsilon_L(\lambda)$, and $\epsilon_M(\lambda)$, respectively, as in expression 2. The bold lines are calculated from the average matrix elements in Table 2; the shaded areas are between two spectra calculated with all of the matrix values set to the averages plus the standard deviations and the averages minus the standard deviations. For the M spectra, this range was too narrow to illustrate. In each panel the spectrum of bacteriorhodopsin is also included.

The entire analysis was repeated for difference spectra measured at 5 and 25°C. In these data sets the strong temperature dependencies of the rate constants of the reactions (35) will have changed the proportions of the intermediates at each sampling time, and therefore the calculated arrays of A were numerically different from one another. In spite of this, the final calculated spectra for K, L, and M from data at the three temperatures are similar to one another (averages shown in Fig. 9, *A–C*). The maxima for K, L, and M are 589–597 nm, 542–544 nm, and 403–405 nm, and their amplitudes relative to that of bacteriorhodopsin are 0.91–0.95, 0.73–0.76, and 0.78–0.80, respectively. These agree well with our earlier derived spectra for K, L, and M (23).

TABLE 2 Location and distribution of the solution space represented by matrix A for measured data for D96N bacteriorhodopsin after each of three filters that eliminate solutions with invalid spectra*

	First filter	Second filter	Third filter
a_{11}	0.775 ± 0.121	0.866 ± 0.099	0.641 ± 0.033
a_{13}	0.064 ± 0.049	0.007 ± 0.009	0.000 ± 0.000
a_{21}	0.083 ± 0.038	0.091 ± 0.038	0.070 ± 0.027
a_{23}	0.244 ± 0.086	0.249 ± 0.014	0.260 ± 0.000
a_{31}	0.007 ± 0.010	0.008 ± 0.010	0.003 ± 0.007
a_{33}	0.796 ± 0.026	0.800 ± 0.000	0.800 ± 0.000
N_s‡	6,912	286	18

* Since any one of the columns in matrix A is determined by the other two (Eq. 5), a_{i2} is left out of the table. Data from 15°C.
‡ Number of solutions.

Calculating the time-dependent concentrations of the intermediates and testing kinetic models

The measured difference spectra at the three temperatures (in Fig. 6 for 15°C; not shown for 5 and 25°C) were fitted with sums of the component difference spectra cal-

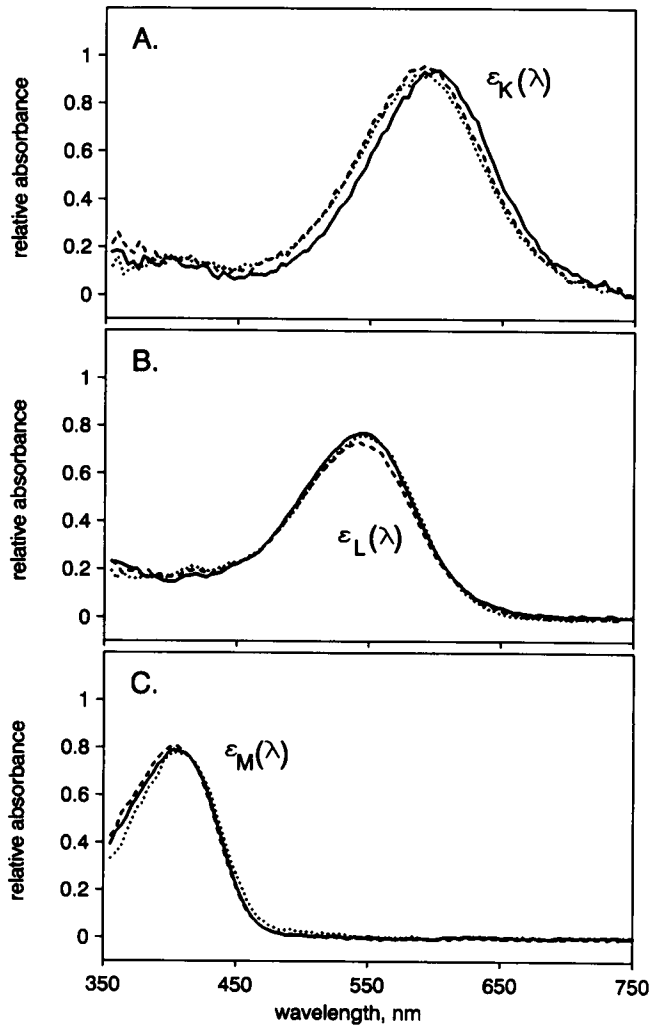

FIGURE 9 Spectra for K, L, and M calculated from data at 5, 15, and 25°C. The spectra are designated as $\epsilon_K(\lambda)$, $\epsilon_L(\lambda)$, and $\epsilon_M(\lambda)$, respectively, as in expression 2. Only spectra calculated from the matrix element averages after the third filter are shown. *Dotted lines*, spectra from 5°C; *solid lines*, spectra from 15°C; *dashed lines*, spectra from 25°C.

culated from the averages in Fig. 8, *A–C*, by subtracting the spectrum of bacteriorhodopsin. At each temperature, the set of spectra calculated at that temperature was used. The time-dependent concentrations of K, L, and M obtained in this way are shown in Fig. 10 (*symbols*). A problem with these fits was indicated by the fact that the sum of the concentrations consistently deviated by up to ~5%, negatively between 1 and 30 μs, and positively between 50 and 500 μs, from 1 (not shown). Because in this time-domain L dominates the deviations of the sum of concentrations from 1 were added to [L] in calculating the points in Fig. 10.

Simple kinetic schemes that might fit such data are of three kinds: (*a*) a single unbranched photocycle with reverse reactions, (*b*) several parallel photocycles originating from heterogeneity of the initial bacteriorhodopsin, with unidirectional steps having different rate constants in each cycle, and (*c*) a single branched photocycle with reverse reactions. Alternative *a* in the form, K ↔ L ↔ M_1 → M_2 → BR, fits the data, except for a persistent pattern of deviation in the concentrations of K and L and L and M from the model just before the maximal amounts of L and M were reached, respectively (Fig. 10). The deviations are not large, but a survey of possible revisions of the model turned up one that eliminated them virtually completely: two L substates with somewhat different spectra, the first where L is in the present scheme and the second in a cul-de-sac equilibrium with

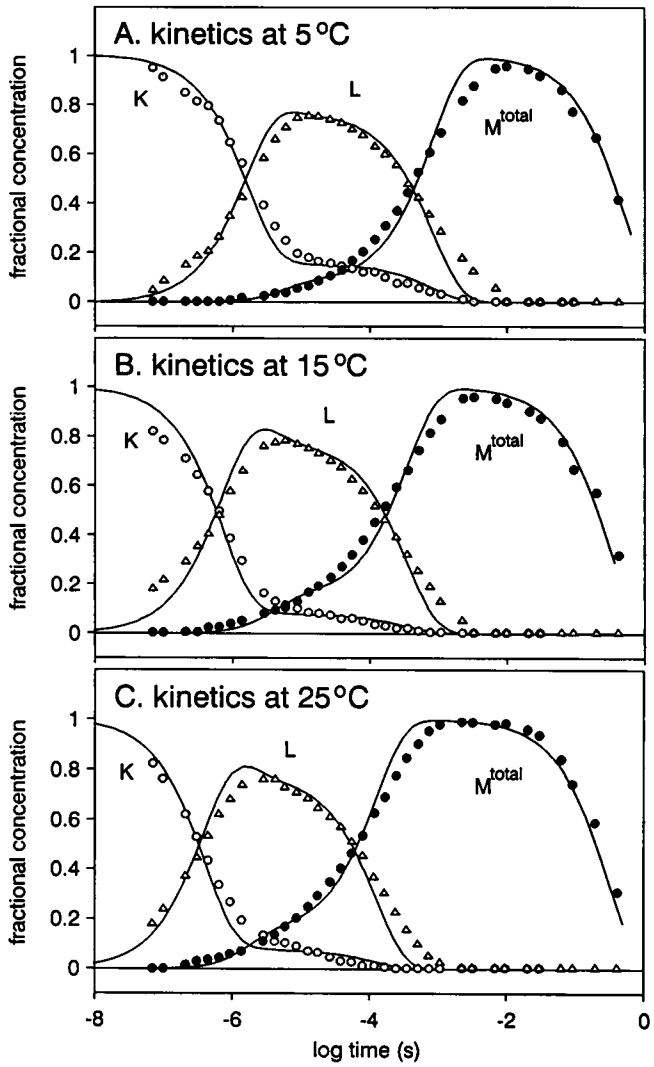

FIGURE 10 Time-resolved concentrations of K, L, and M and fits of a kinetic model at 5°C (*A*), 15°C (*B*), and 25°C (*C*). Symbols: ○, K; △, L; ●, M^{total} (i.e., M_1 + M_2). The points were calculated by fitting weighted sums of difference spectra based on the spectra in Fig. 9 at each temperature to the measured spectra. The lines are the best fits of the model K ↔ L ↔ M_1 → M_2 → BR. The rate constants are the following (the three values, given in s^{-1}, refer to 5, 15, and 25°C, respectively): k_{KL}, 5.0×10^6, 1.25×10^7, 2.22×10^7; k_{LK}, 1.0×10^6, 1.25×10^6, 2.22×10^6; k_{LM1}, 2.3×10^4, 4.55×10^4, 1.11×10^5; k_{M1L}, 2.0×10^5, 2.13×10^5, 5.0×10^5; k_{M1M2}, 1.43×10^4, 1.82×10^4, 5.0×10^4; k_{M2BR}, 2.0, 3.3, 3.3.

M_1 (not shown). Two L states with different spectra would account also for the deviations in the sums of concentrations. In view of the fact that the search that had produced the spectra was independent of a kinetic model, we consider the fits in Fig. 10 a good first approximation. However, further refinement of the linear model, such as the introduction of a second L state, will be necessary, and we are at present exploring the various options.

Alternative *b* had been proposed on the basis of many observations of two or three time constants for the rise of M (12, 14, 17, 18). In these models the amplitudes of the kinetic components are regarded as the fractions of bacteriorhodopsin subpopulations that originate the parallel photocycles, and each of the multiple time constants for a reaction is assigned to a separate photocycle. However, fitting the data to the simplest of these models, that of two parallel photocycles each with a K → L → M sequence, gave unacceptable results (Fig. 11 *A*). The problem is that the amplitudes in one transition do not match the amplitudes in the other. As Fig. 11 *A* shows, when the K to L reaction is resolved into the independent components, the ratio of these components (9:1 in this case) does not allow the fitting of the rise of M with two components because that would require a ratio closer to unity. Similarly, resolving the rise of M instead (not shown) would have given very poor fit for the K to L transition. More complicated versions of such models, including those with more than two photocycles, reverse reactions, and with some of the photocycles lacking one or another intermediate, would presumably give adequate fits, however.

On the other hand, alternative *c* does produce a satisfactory fit to the points when in the form K ↔ L → M_2 plus the cul-de-sac L ↔ M_1 (Fig. 11 *B*) or particularly in the form L ↔ K ↔ M_1 → M_2, where L is the product of a side reaction (Fig. 11 *C*). Deciding for or against these models cannot be from kinetic evidence only but on the basis of mechanistic and structural considerations of the physical processes that take place during the chromophore transformations.

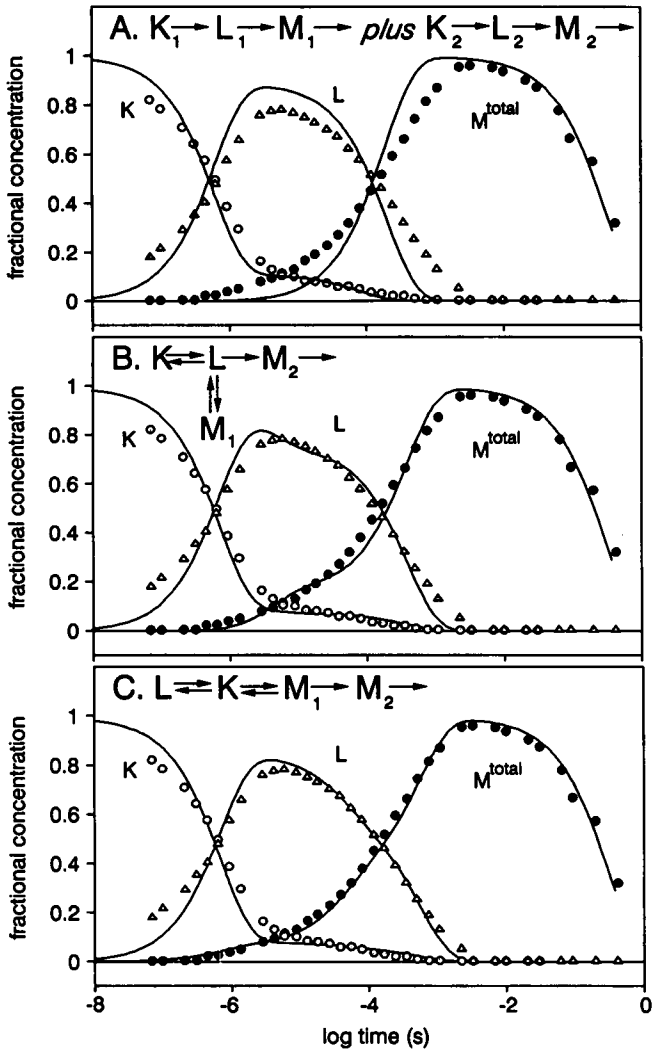

FIGURE 11 Time-resolved concentrations of K, L, and M and fits of three different kinetic models other than the single sequential scheme in Fig. 10. Symbols: ○, K; △, L; ●, M^{total} (i.e., $M_1 + M_2$). The points were calculated by fitting weighted sums of difference spectra based on the spectra in Fig. 9 at 15°C to the measured spectra. The lines are the best fits of a model with two parallel photocycles, i.e., $K_1 \rightarrow L_1 \rightarrow M_1 \rightarrow$ plus $K_2 \rightarrow L_2 \rightarrow M_2 \rightarrow$ (*A*); a model with a branch at L, i.e., K ↔ L → M_2 → plus L ↔ M_1 (*B*); and a model with a branch at K, i.e., L ↔ K ↔ M_1 → M_2 → (*C*). The rate constants are the following: (*A*) $k_{K1L1} = 1.67 \times 10^6$, $K_{L1M1} = 5.0 \times 10^3$, $k_{M1BR} = 3.33$, $k_{K2L2} = 1.25 \times 10^4$, $k_{L2M2} = 5.0 \times 10^5$, $k_{M2BR} = 3.33$, ratio of the two initial amplitudes 89:11; (*B*) $k_{KL} = 1.25 \times 10^6$, $k_{LK} = 1.25 \times 10^5$, $k_{LM2} = 3.33 \times 10^3$, $k_{LM1} = 4.55 \times 10^4$, $k_{M1L} = 2.13 \times 10^5$, $k_{M2BR} = 3.33$; (*C*) $k_{LK} = 1.25 \times 10^6$, $k_{KL} = 1.25 \times 10^5$, $k_{KM1} = 1.0 \times 10^5$, $k_{M1K} = 1.25 \times 10^4$, $k_{M1M2} = 5.0 \times 10^3$, $k_{M2BR} = 3.33$.

DISCUSSION

We used a set of time-dependent difference spectra in the D96N bacteriorhodopsin photocycle to generate all mathematically possible solutions for the spectra of the intermediates K, L, and M. The solutions were represented by a six-dimensional array that contained the corresponding intermediate concentrations. At a grid resolution consistent with reasonable signal to noise ratio, the array represents a very large number of points, most of which do not correspond to valid spectra and can be eliminated. It is important to emphasize that in this approach the spectra were calculated without regard of a photocycle model. Some of the calculated spectra were objectively invalid because they contained negative amplitudes, whereas others were deemed invalid because they did not correspond to what is known, empirically and from theoretical considerations, about the shape of the visible band of rhodopsins. We applied independent and progressively stringent restricting criteria of this kind ("filters") and evaluated their effects on the number, average and standard deviation, and the spatial distribution of the solutions. The validity of this kind of

analysis depends on the validity of the criteria. If the criteria are valid, then the calculation is valid, because grid search of simulated data constructed from known spectra demonstrated that the procedure converges to spectra in good agreement with the known input spectra. Importantly, we found that not accepting grid points that gave negative absorptions and more than one peak for M returned already a good approximation of the input spectra (Fig. 4 *A*). The rest of the criteria merely decreased the uncertainty in this solution (Table 1 and Figs. 3 and 4).

The calculations with measured data from the D96N protein indicated that, as with the simulated data, the averages of the matrix elements of the solutions remained within about one standard deviation as independent and increasingly restrictive filters were used. What was mostly affected was the size of the solution space (Table 2). Thus, for the measured data also, even the simplest and most defensible of the restricting criteria, that of allowing only positive absorptions and a single peak for the M intermediate, generated solutions with average array values corresponding to spectra similar to the final ones. We conclude that in both simulated and real data the solution space is distributed densely around the singular ultimate solution already after the first filter, and applying further restrictive filters eliminates primarily those solutions that lie farther from this point.

The result of the calculations with measured data is a set of spectra for K, L, and M with standard deviations of a few percent in the amplitudes and uncertainties of a few nanometers in the wavelength of the maxima. The spectra are very similar when calculated from data sets obtained at different temperatures (5, 15, and 25°C) containing different spectral mixtures. Calculation of the time-dependent concentrations of K, L, and M (M_1 + M_2) with these spectra produced kinetics consistent with the scheme proposed earlier (23); K ↔ L ↔ M_1 → M_2 → BR. Small and consistent deviations indicated that this scheme overlooks some complication between L and M_1. The cause of the discrepancies is probably an additional L state with somewhat different spectrum from the initial L, but this idea needs further support. As in any kinetic study, more complicated models with more than one photocycles and/or branches would certainly fit the data within error. Nevertheless, the results indicate that the K ↔ L ↔ M_1 → M_2 scheme explains the data reasonably well; it is the simplest workable model for the first part of the bacteriorhodopsin photocycle.

We are grateful to K. Schulten and R. Birge for advice on how the electronic states of retinal define the absorption spectra.

This work was supported by grants from the National Institutes of Health (GM-29498) and the National Aeronautics and Space Administration (NAGW-212).

Received for publication 17 June 1992 and in final form 25 August 1992.

REFERENCES

1. Mathies, R. A., S. W. Lin, J. B. Ames, and W. T. Pollard. 1991. From femtoseconds to biology: mechanism of bacteriorhodopsin's light-driven proton pump. *Annu. Rev. Biophys. Biophys. Chem.* 20:491–518.
2. Braiman, M. S., and R. A. Mathies. 1982. Resonance Raman spectra of bacteriorhodopsin's primary photoproduct: evidence for a distorted 13-*cis* retinal chromophore. *Proc. Natl. Acad. Sci. USA.* 79:403–407.
3. Siebert, F., and W. Mantele. 1983. Investigation of the primary photochemistry of bacteriorhodopsin by low-temperature Fourier-transform infrared spectroscopy. *Eur. J. Biochem.* 130:565–573.
4. Smith, S. O., J. A. Pardoen, P. P. J. Mulder, B. Curry, J. Lugtenburg, and R. A. Mathies. 1983. Chromophore structure in bacteriorhodopsin's O_{640} photointermediate. *Biochemistry.* 22:6141–6148.
5. Braiman, M. S., T. Mogi, T. Marti, L. J. Stern, H. G. Khorana, and K. J. Rothschild. 1988. Vibrational spectroscopy of bacteriorhodopsin mutants: light-driven proton transport involves protonation changes of aspartate residues 85, 96, and 212. *Biochemistry.* 27:8516–8520.
6. Gerwert, K., B. Hess, J. Soppa, and D. Oesterhelt. 1989. Role of aspartate-96 in proton translocation by bacteriorhodopsin. *Proc. Natl. Acad. Sci. USA.* 86:4943–4947.
7. Butt, H.-J., K. Fendler, E. Bamberg, J. Tittor, and D. Oesterhelt. 1989. Aspartic acids 96 and 85 play a central role in the function of bacteriorhodopsin as a proton pump. *EMBO (Eur. Mol. Biol. Organ.) J.* 8:1657–1663.
8. Tittor, J., C. Soell, D. Oesterhelt, H.-J. Butt, and E. Bamberg. 1989. A defective proton pump, point-mutated bacteriorhodopsin Asp96 → Asn is fully reactivated by azide. *EMBO (Eur. Mol. Biol. Organ.) J.* 8:3477–3482.
9. Stern, L. J., P. L. Ahl, T. Marti, T. Mogi, M. Duñach, S. Berkovitz, K. J. Rothschild, and H. G. Khorana. 1989. Substitution of membrane-embedded aspartic acids in bacteriorhodopsin causes specific changes in different steps of the photochemical cycle. *Biochemistry.* 28:10035–10042.
10. Pfefferlé, J.-M., A. Maeda, J. Sasaki and T. Yoshizawa. 1991. Fourier transform infrared study of the N intermediate of bacteriorhodopsin. *Biochemistry.* 30:6548–6556.
11. Lozier, R. H., R. A. Bogomolni, and W. Stoeckenius. 1975. Bacteriorhodopsin: a light-driven proton pump in *Halobacterium halobium*. *Biophys. J.* 15:955–963.
12. Hanamoto, J. H., P. Dupuis, and M. A. El-Sayed. 1984. On the protein (tyrosine)-chromophore (protonated Schiff base) coupling in bacteriorhodopsin. *Proc. Natl. Acad. Sci. USA.* 81:7083–7087.
13. Groma, G. I., and Z. Dancsházy. 1986. How many M forms are there in the bacteriorhodopsin photocycle?. *Biophys. J.* 50:357–366.
14. Dancsházy, Z., R. Govindjee, and T. G. Ebrey. 1988. Independent photocycles of the spectrally distinct forms of bacteriorhodopsin. *Proc. Natl. Acad. Sci. USA.* 85:6358–6361.
15. Liu, S. Y. 1990. Light-induced currents from oriented purple membrane. I. Correlation of the microsecond component (B2) with the L–M photocycle transition. *Biophys. J.* 57:943–950.
16. Balashov, S. P., R. Govindjee, and T. G. Ebrey. 1991. Red shift of the purple membrane absorption band and the deprotonation of tyrosine residues at high pH. Origin of the parallel photocycles of *trans*-bacteriorhodopsin. *Biophys. J.* 60:475–490.
17. Diller, R., and M. Stockburger. 1988. Kinetic resonance Raman studies reveal different conformational states of bacteriorhodopsin. *Biochemistry.* 27:7641–7651.

18. Bitting, H. C., D.-J. Jang, and M. A. El-Sayed. 1990. On the multiple cycles of bacteriorhodopsin at high pH. *Photochem. Photobiol.* 51:593–598.

19. Sherman, W. V., R. Korenstein, and S. R. Caplan. 1976. Energetics and chronology of phototransients in the light response of the purple membrane of *Halobacterium halobium*. *Biochim. Biophys. Acta.* 430:454–458.

20. Butt, H.-J., K. Fendler, A. Dér, and E. Bamberg. 1989. Temperature jump study of charge translocation during the bacteriorhodopsin photocycle. *Biophys. J.* 56:851–859.

21. Chernavskii, D. S., I. V. Chizhov, R. H. Lozier, T. M. Murina, A. M. Prokhorov, and B. V. Zubov. 1989. Kinetic model of bacteriorhodopsin photocycle: pathway from M state to bR. *Photochem. Photobiol.* 49:649–653.

22. Váró, G., and J. K. Lanyi. 1990. Pathways of the rise and decay of the M photointermediate of bacteriorhodopsin. *Biochemistry.* 29:2241–2250.

23. Váró, G., and J. K. Lanyi. 1991. Kinetic and spectroscopic evidence for an irreversible step between deprotonation and reprotonation of the Schiff base in the bacteriorhodopsin photocycle. *Biochemistry.* 30:5008–5015.

24. Gerwert, K., G. Souvignier, and B. Hess. 1990. Simultaneous monitoring of light-induced changes in protein side-group protonation, chromophore isomerization, and backbone motion of bacteriorhodopsin by time-resolved Fourier-transform infrared spectroscopy. *Proc. Natl. Acad. Sci. USA.* 87:9774–9778.

25. Otto, H., T. Marti, M. Holz, T. Mogi, M. Lindau, H. G. Khorana, and M. P. Heyn. 1989. Aspartic acid-96 is the internal proton donor in the reprotonation of the Schiff base of bacteriorhodopsin. *Proc. Natl. Acad. Sci. USA.* 86:9228–9232.

26. Ames, J. B., and R. A. Mathies. 1990. The role of back-reactions and proton uptake during the N → O transition in bacteriorhodopsin's photocycle: a kinetic resonance Raman study. *Biochemistry.* 29:7181–7190.

27. Kouyama, T., A. Nasuda-Kouyama, A. Ikegami, M. K. Mathew, and W. Stoeckenius. 1988. Bacteriorhodopsin photoreaction: identification of a long-lived intermediate N (P, R_{350}) at high pH and its M-like photoproduct. *Biochemistry.* 27:5855–5863.

28. Nagle, J. F. 1991. Solving complex photocycle kinetics. Theory and direct method. *Biophys. J.* 59:476–487.

29. Xie, A. H., J. F. Nagle, and R. H. Lozier. 1987. Flash spectroscopy of purple membrane. *Biophys. J.* 51:627–635.

30. Maurer, R., J. Vogel, and S. Schneider. 1987*a*. Analysis of flash photolysis data by a global fit with multiexponentials. I. Determination of the minimal number of intermediates in the photocycle of bacteriorhodopsin by the "stability criterion." *Photochem. Photobiol.* 46:247–253.

31. Maurer, R., J. Vogel, and S. Schneider. 1987*b*. Analysis of flash photolysis data by a global fit with multiexponentials. II. Determination of consistent natural rate constants and the absolute spectra of the transient species in the bacteriorhodopsin photocycle from measurements at different temperatures. *Photochem. Photobiol.* 46:255–261.

32. Milder, S. J., T. E. Thorgeirsson, L. J. W. Miercke, R. M. Stroud, and D. S. Kliger. 1991. Effects of detergent environments on the photocycle of purified monomeric bacteriorhodopsin. *Biochemistry.* 30:1751–1761.

33. Thorgeirsson, T. E., S. J. Milder, L. J. W. Miercke, M. C. Betlach, R. F. Shand, R. M. Stroud, and D. S. Kliger. 1991. Effects of Asp-96 → Asn, Asp-85 → Asn, and Arg-82 → Gln single-site substitutions on the photocycle of bacteriorhodopsin. *Biochemistry.* 30:9133–9142.

34. Müller, K.-H., H. J. Butt, E. Bamberg, K. Fendler, B. Hess, F. Siebert, and M. Engelhard. 1991. The reaction cycle of bacteriorhodopsin: an analysis using visible absorption, photocurrent and infrared techniques. *Eur. Biophys. J.* 19:241–251.

35. Váró, G., and J. K. Lanyi. 1991. Thermodynamics and energy coupling in the bacteriorhodopsin photocycle. *Biochemistry.* 30:5016–5022.

36. Lozier, R. H., A. Xie, J. Hofrichter, and G. M. Clore. 1992. Reversible steps in the bacteriorhodopsin photocycle. *Proc. Natl. Acad. Sci. USA.* 89:3610–3614.

37. Váró, G., and J. K. Lanyi. 1991. Distortions in the photocycle of bacteriorhodopsin at moderate dehydration. *Biophys. J.* 59:313–322.

38. Oesterhelt, D., and W. Stoeckenius. 1974. Isolation of the cell membrane of *Halobacterium halobium* and its fractionation into red and purple membrane. *Methods Enzymol.* 31:667–678.

39. Cao, Y., G. Váró, M. Chang, B. Ni, R. Needleman, and J. K. Lanyi. 1991. Water is required for proton transfer from aspartate 96 to the bacteriorhodopsin Schiff base. *Biochemistry.* 30:10972–10979.

40. Zimányi, L., L. Keszthelyi, and J. K. Lanyi. 1989. Transient spectroscopy of bacterial rhodopsins with optical multichannel analyzer. 1. Comparison of the photocycles of bacteriorhodopsin and halorhodopsin. *Biochemistry.* 28:5165–5172.

41. Birge, R. R., K. Schulten, and M. Karplus. 1975. Possible influence of a low-lying "covalent" excited state on the absorption spectrum and photoisomerization of 11-*cis* retinal. *Chem. Phys. Lett.* 31:451–454.

42. Becher, B., F. Tokunaga, and T. G. Ebrey. 1978. Ultraviolet and visible absorption spectra of the purple membrane protein and the photocycle intermediates. *Biochemistry.* 17:2293–2300.

43. Schulten, K., U. Dinur, and B. Honig. 1980. The spectra of carbonium ions, cyanine dyes, and protonated Schiff base polyenes. *J. Chem. Phys.* 73:3927–3935.

44. Crescitelli, F. 1977. Ionochromic behavior of Gecko visual pigments. *Science (Wash. DC).* 195:187–188.

45. Steiner, M., and D. Oesterhelt. 1983. Isolation and properties of the native chromoprotein halorhodopsin. *EMBO (Eur. Mol. Biol. Organ.) J.* 2:1379–1385.

46. Shichida, Y., S. Matuoka, Y. Hidaka, and T. Yoshizawa. 1983. Absorption spectra of intermediates of bacteriorhodopsin measured by laser photolysis at room temperatures. *Biochim. Biophys. Acta.* 723:240–246.

47. Hug, S. J., J. W. Lewis, C. M. Einterz, T. E. Thorgeirsson, and D. S. Kliger. 1990. Nanosecond photolysis of rhodopsin: evidence for a new, blue-shifted intermediate. *Biochemistry.* 29:1475–1485.

48. Straume, M., D. C. Mitchell, J. L. Miller, and B. J. Litman. 1990. Interconversion of metarhodopsins I and II: a branched photointermediate decay model. *Biochemistry.* 29:9135–9142.

49. Golub, G., and W. Kahan. 1965. Calculating the singular values and pseudo-inverse of a matrix. *SIAM J. Num. Anal.* 2:205–224.